Unveiling biological activities of biosynthesized starch/silver-selenium nanocomposite using *Cladosporium cladosporioides* CBS 174.62

Fathy M. Elkady[1], Amr H. Hashem[2], Salem S. Salem[2]* , Gharieb S. El-Sayyad[3,4,5]*, Ahmed Abdel Tawab[6], Mohammad M. Alkherkhisy[6] and Mohammed S. Abdulrahman[1]

Abstract

Background and objectives Microbial cells capability to tolerate the effect of various antimicrobial classes represent a major worldwide health concern. The flexible and multi-components nanocomposites have enhanced physico-chemical characters with several improved properties. Thus, different biological activities of biosynthesized starch/silver-selenium nanocomposite (St/Ag-Se NC) were assessed.

Methodology The St/Ag-Se NC was biosynthesized using *Cladosporium cladosporioides* CBS 174.62 (*C. cladosporioides*) strain. The shape and average particle size were investigated using scanning electron microscope (SEM) and high-resolution transmission electron microscope (HR-TEM), respectively. On the other hand, the St/Ag-Se NC effect on two cancer cell lines and red blood cells (RBCs) was evaluated and its hydrogen peroxide (H_2O_2) scavenging effect was assessed. Moreover, its effects on various microbial species in both planktonic and biofilm growth forms were examined.

Results The St/Ag-Se NC was successfully biosynthesized with oval and spherical shape and a mean particle diameter of 67.87 nm as confirmed by the HR-TEM analysis. St/Ag-Se NC showed promising anticancer activity toward human colorectal carcinoma (HCT-116) and human breast cancer (MCF-7) cell lines where IC_{50} were 21.37 and 19.98 µg/ml, respectively. Similarly, little effect on RBCs was observed with low nanocomposite concentration. As well, the highest nanocomposite H_2O_2 scavenging activity (42.84%) was recorded at a concentration of 2 mg/ml. Additionally, *Staphylococcus epidermidis* (*S. epidermidis*) ATCC 12,228 and *Candida albicans* (*C. albicans*) ATCC 10,231 were the highly affected bacterial and fungal strains with minimum inhibitory concentrations (MICs) of 18.75 and 50 µg/ml, respectively. Moreover, the noticeable effect of St/Ag-Se NC on microbial biofilm was concentration dependent. A high biofilm suppression percentage, 87.5% and 68.05%, were recorded with *S. epidermidis* and *Staphylococcus aureus* (*S. aureus*) when exposed to 1 mg/ml and 0.5 mg/ml, respectively.

Conclusion The biosynthesized St/Ag-Se NC showed excellent antioxidant activity, haemocompatibility, and anti-proliferative effect at low concentrations. Also, it exhibited promising antimicrobial and antibiofilm activities.

*Correspondence:
Salem S. Salem
salemsalahsalem@azhar.edu.eg
Gharieb S. El-Sayyad
Gharieb.S.Elsayyad@eaea.org.eg
Full list of author information is available at the end of the article

Elkady *et al. BMC Microbiology*   (2024) 24:78

Page 2 of 17

Introduction

Antimicrobial resistance has emerged as a significant global health concern during the past twenty years [1]. Antimicrobial resistance is the capacity of a bacterium to withstand the impact of different antimicrobial agents. In this specific manifestation of resistance, bacteria possess the capacity to endure the impacts of medication that was formerly efficacious against them [2]. Multidrug resistance (MDR) is the occurrence of resistance to numerous medicines. Microorganisms possess a variety of resistance mechanisms, including innate resistance exhibited by particular microorganisms against certain antimicrobial agents, genetic changes, and acquired resistance acquired from other species [3]. The misuse of antibiotics has resulted in the emergence of numerous multidrug-resistant microorganisms [4, 5]. Another issue is cancer, which due to its high mortality rate, has risen to become a global health crisis of the twenty-first century. Every year, nearly 15 million people lose their lives because of lingering cancer cells [6]. Numerous chemotherapeutic medicines are already available for treating malignancies, but they all have significant negative effects on various human organs [7]. Thus, many of scientists have turned to use safe alternative to antimicrobial and anticancer drugs.

Nanotechnology have received much attention in the last period where have been used in medicine, pharmaceutical, chemistry and agriculture fields [8–15]. Nanoparticles (NPs) are defined as particles ranging from 1 to 100 nm in size [16, 17]. Their small size gives rise to a diverse range of atomic-level features [18–20]. Biopolymers are a big and promising group of polymers that have benefits like being biocompatible, biodegradable, and low in toxicity [21–23]. Starch is a consumable polysaccharide that finds application in several biological, nutritional, and food processing industries [24]. In addition, starch is employed as a reducing agent in the process of manufacturing copper NPs, which are then stabilized by chitosan polymers. Artificial implants utilize their antibacterial properties to serve as a covering that promotes wound healing [25]. Nanocomposites are novel materials that exhibit enhanced flexibility, as well as improved physical and chemical properties. These materials are characterized by their multifunctionality, as they are composed of several polymers [26]. Herein, this study aimed to evaluate the in vitro cytotoxicity of biosynthesized triple-component St/Ag-Se NC, identify its hemolytic and antioxidant activities, clarify its effect on microbial cell wall, and assess the destructive activity of these nanocomposite on both planktonic and biofilm forms of various bacterial as well as fungal strains.

Materials and methods

Biological synthesis of St/Ag-Se NC

Preparation of Cladosporium culture

One loop from *C. cladosporioides* culture, supplied from the Regional Center for Mycology and Biotechnology (RCMB), Al Azhar university, Cairo, Egypt, was grown in Sabouraud dextrose agar (SDA) and incubated 7 days. The *C. cladosporioides* was inoculated in 500 ml of double strength liquid malt extract medium with a pH of 5.6 in a 1000 ml Erlenmeyer flask and incubated stationary at 28 °C for 7 days [27].

Synthesis of St/Ag-Se NC

After being cleaned with sterile water, the 10 gm mass cell of *C. cladosporioides* was reintroduced in 100 mL of purified water and incubated for one day at 28 °C and 120 rpm. The following procedure was utilised to create Ag-Se NPs after filtering the *C. cladosporioides* cell-free filtrate: For 24 h at 28 °C and 120 rpm, 2.0 mM silver nitrate and 2.0 mM sodium selenate were added to 100 mL of *C. cladosporioides* filtrate [28]. A deep brown color that developed in the cell-free filtrate implied Ag-Se NP production. Then, 400 mg of soluble starch was added, and the mixture was stirred for 60 min with a magnetic stirrer to create a mixture that covered silver-selenium nanocomposite (St/Ag-Se NC). The sample was dried in the oven at 120 °C for 24 h to obtain the product in a powder state in order to facilitate its use in further investigation.

Characterization of St/Ag-Se NC

Using a UV-Vis. spectrophotometer (JASCO V-560) at certain wavelengths, the absorbance and optical properties of produced St/Ag-Se NC were examined. For Auto-zero reasons, a sample devoid of any metal ions was additionally included. All samples were initially screened for optical characteristics and to establish the fixed wavelengths used to calculate absorbance. As well, crystal structure and phase of the prepared St/Ag-Se NC were analyzed using X-ray diffraction analysis (XRD) analysis [29, 30]. Using the XRD-6000 lists, Shimadzu equipment, SSI, Japan, it was possible to assess the crystallization, crystallite size, and/or structure of the generated St/Ag-Se NC. The magnitude of the diffracted X-rays was measured using the diffracted angle 2θ [31]. To ascertain the mean size distribution of the

Elkady *et al. BMC Microbiology*   (2024) 24:78

Page 3 of 17

produced NPs, measurements of dynamic light scattering (DLS) were made at the St. Barbara, California, USA facility using the DLS-PSS-NICOMP 380-ZLS particles sized system. One hundred microlitters of St/Ag-Se NC specimens were transferred to a temporary, tiny cuvette. Five procedures were carried out after equilibration at a temperature of 25 ± 2 °C for 2.0 min [32]. In addition, at the pH of synthesis, the surface charges of the biosynthesized St/Ag-Se NC were indirectly evaluated using a Malvern device Zeta potential analyzer, UK [31]. To clarify surface shape, border size, and the distribution of the generated St/Ag-Se NC surrounding starch, an analysis using SEM (ZEISS, EVO-MA10, Germany) was performed [33]. Finally, the shape, appearance, and average particle size of the produced St/Ag-Se NC were investigated using a HR-TEM (JEM2100, Jeol, Japan). St/Ag-Se NC sample used for TEM studies were drop-coated into carbon-coated TEM grids following dried in an incubator at 37.0 ± 2 °C [34].

Evaluation of St/Ag-Se NC anti-proliferative effect

The 3-(4,5-dimethylthiazol-2-yl)-2,5-diphenyletetrazolium bromide (MTT) cytotoxicity assay was performed on HCT-116 and MCF-7 cancer cell lines using doxorubicin and imatinib as a control, respectively. This colorimetric assay evaluates cells proliferation based on the ability of live cells to enzymatically metabolize the MTT soluble salt to its insoluble purple formazan form that can be quantified spectrophotometrically at 570 nm [35]. Cells were detached from the T-75 flasks by addition of 1 ml trypsin/EDTA solution per flask and subsequently incubated for 3 min at 37 °C. Detached cells were then re-suspended in 10 ml complete growth medium, transferred to 15 ml Falcon tube, and centrifuged at 1000 rpm for 3 min to remove trypsin. The cell pellet was re-suspended in 10 ml growth medium with gentle agitation for well mixing. Using micropipette, 10 μl of cells suspension were placed on Hemocytometer to determine cell number using the inverted microscope. Using a handtally counter, the number of cells in this area of 16 squares was counted. The Hemocytometer was moved to another set of 16 corner squares and counting was carried on until all 4 corners squares were counted. The Hemocytometer is designed so that the number of cells in one set of 16 corner is equivalent to the number of cells X 10^4. Therefore, once the total cell count has been obtained, the cell concentration (cell/ml) can be calculated as the following:

The cells suspension was diluted by complete medium to a concentration of 5×10^4 cell/ml and 100 μl were pipetted into each well of 96 well plate (about 5000 cell/well) followed by incubation at 37 °C for 24 h to allow cells attachment. Cells were then treated with 100 μl of growth medium contains 0, 0.001, 0.01, 0.1, 1, 10, 100 and 1000 μg/ml of the tested nanocomposite in triplicate. After 72 h, media were removed from wells, 100 μl of MTT solution were added to each well, and incubated for 2 h at 37 °C. The excess MTT was then removed, 100 μl acidified isopropanol were added to each well, and the plates were incubated at 37 °C for 30 min with continuous shaking to dissolve the formed crystals. The developed purple color, that reflect the cells viability, was determined spectrophotometrically using Epoc-2 C micro-plate reader (BioTek, USA) at 570 nm. Results were expressed in terms of inhibition concentration fifty (IC_{50}), the concentration required to inhibit cell growth by 50% relative to nanocomposite untreated cells, which calculated using Graph Pad Prism version 8.01, 2015 (GraphPad software, San Diego, USA). Through generating dose response curve by plotting the log concentration versus corresponding viability percentage [36].

Assessment of St/Ag-Se NC hemolytic effect

The hemolytic activity of the biosynthesized nanocomposite was then examined as described by [37]: Briefly, 4 ml of fresh blood from healthy human were collected in EDTA tube, mixed with 8 ml of 0.2 M (Dulbecco's) D-phosphate-buffered saline (D-PBS) solution (pH = 7), and centrifuged for 10 min at 10,000 rpm at 4 °C (for serum separation). For further rinsing, the RBCs in the pellet were resuspended in 8 ml phosphate buffer saline (PBS) followed by centrifugation at 10,000 rpm for 10 min. The obtained RBCs pellet was then suspended using 40 ml D-PBS. This suspension was divided into 3 parts, the 1st one or test sample subjected to the biosynthesized St/Ag-Se NC at different concentrations [0.25, 0.5, 1, and 2 mg/ml], the 2nd part was treated with triton X-100 (0.1% v/v) as a positive control, while the 3rd part was exposed to PBS as a negative control. All samples were incubated for 4 h at room temperature followed by vortex and centrifugation for 3 min at 10,000 rpm. In microtiter plate, for each 200 μl of the collected supernatant, the

$$\text{Total cell count } = \frac{\text{Total cells counted in 4 squares}}{\text{Number of squares}} \times 10^4 \text{ (cell/ml)}$$

Elkady *et al. BMC Microbiology*   (2024) 24:78

Page 4 of 17

optical density (OD) was detected at 540 nm using an ELISA plate reader. The hemolysis percentages were then calculated as following:

$$\% \textbf{ Hemolysis } \% = \frac{\textbf{Mean OD of test sample} - \textbf{Mean OD of negative control}}{\textbf{Mean OD of positive control} - \textbf{Mean OD of negative control}} \times 100$$

Detection of St/Ag-Se NC antioxidant activity

Hydrogen peroxide scavenging activity was performed to assess the St/Ag-Se NC antioxidant effect according to [38]. The experiment involved mixing 100 µl of the tested nanocomposite at concentrations of 0.5, 1, or 2 mg/ml with 0.3 ml of PBS (50 mM, pH = 7.4) and 0.6 ml of H_2O_2 solution (2 mM H_2O_2 in PBS, 50 mM, pH = 7.4). The solution was subjected to vortexing, and the absorbance at a wavelength of 230 nm was measured using a UV–Vis spectrophotometer (Systronics, AU-2701) after a duration of 10 min. Ascorbic acid served as the standard, whereas PBS (50 mM, pH = 7.4) was utilized as the blank. The H_2O_2 scavenging activity was quantified by calculating the percentage using the following formula:

$$\textbf{Scavenging } \% = \frac{\text{Ac} - \text{As}}{\text{Ac}} \times \textbf{100}$$

Where Ac represents the absorbance of control (using PBS instead of the test sample) and As absorbance of St/Ag-Se NC or ascorbic acid.

Effect of St/Ag-Se NC on microbial cell membrrane

Potassium (K^+) ions leakage analysis was followed to clarify the St/Ag-Se NC effect on microbial culture. Fifty micolitters of 0.5 McFarland standard turbidity or 1×10^6 spore/ml of bacterial or fungal spore (mold) suspension, respectively were inoculated onto 20 ml of nutrient broth and incubated for 24 h at 37 °C in case of bacteria or sabouraud dextrose broth (SDB) and incubated for 48 h at 28 °C in case of fungi. After centrifugation at 5000 rpm for 10 min, the supernatant discarded while the precipitated cells resuspended in 20 ml saline containing 100 µl of the biosynthesized nanocomposite at concentration 2 mg/ml, and incubated for 16 h at 37 °C. After centrifugation at 5000 rpm for 10 min, the supernatant was collected for determination of the released cytoplasmic K^+ ion concentration using flame photometry. The experimental data were normalized against the data of untreated cell supernatant [control (C)] under the same conditions in absence of St/Ag-Se NC [39].

Primary screening for St/Ag-Se NC antimicrobial activity

The agar well diffusion method was used for preliminary detection of St/Ag-Se NC, sodium selenite, silver nitrate, and starch antimicrobial effects [40]. Standardized concentrations, 0.5 McFarland of each overnight bacterial culture or 1×10^6 spore/ml of each fungal spore suspension, were prepared and swabbed aseptically onto the Mueller-Hinton agar (MHA) plates for bacteria or SDA plates for fungi. Holes of 6 mm were then made on the agar using sterilized cork borer. Fifty microliters of either starch, sodium selenite, silver nitrate, or St/Ag-Se NC were put in each hole under aseptic condition and kept at room temperature for 1 h. Chloramphenicol (30 µg/ml) and fluconazole (50 µg/ml) served as positive control for bacteria and fungi, respectively. The MHA plates were then incubated at 37 °C for 24 h while, the SDA plates were incubated at 28 °C for 48 h followed by inhibition zone diameters (IZDs) measurement [41]. In the current work, the antimicrobial activity of St/Ag-Se NC was assessed against standard strains of some Gram-positive bacteria including *Staphylococcus aureus* (*S. aureus*) ATCC 6538, *S. epidermidis* ATCC 12,228, and *Bacillus subtilus* (*B. subtilus*) ATCC 6633 and some Gram-negative bacteria including *Escherichia coli* (*E. coli*) ATCC 8739, *Pseudomonas aeruginosa* (*P. aeruginosa*) ATCC 9027, *Klebsiella pneumonia (K. pneumonia)* ATCC 13,882, *Proteus mirabilis* (*P. mirabilis*) ATCC 25,933, and *Salmonella typhi* (*S. typhi*) ATCC 14,028. On the other hand, the antifungal activity was assessed against some standard strains of molds including *Aspergillus niger* (A. *niger*) CBS 31.29, *Aspergillus. fumigatus (A. fumigatus)* CBS 106, and *Cladosporium herbarum* (Link) Fr. CBS 813.71 and some *Candida* species including *C. albicans* ATCC 10,231 and *Candida tropicalis* (*C. tropicalis*) ATCC 13,803.

Quantitative antimicrobial tests
Determination of inhibitory concentrations

The St/Ag-Se NC minimum inhibitory concentration (MIC), minimum bactericidal concentration (MBC), and minimum fungicidal concentration (MFC) against selected bacterial and fungal standard strains were determined. Broth microdilution method according to Clinical Laboratory Standard Institute (CLSI) guidelines (2017) was applied for determination of MIC. Briefly, 50 µl of tryptic soya broth (TSB) for bacteria or SDB in case of fungi was added to each well of microtiter plate. In every raw, 50 µl from the prepared stock concentration of St/Ag-Se NC (2 mg/ml) in DMSO was added to the 1st well followed by two-fold serial dilution. Bacterial colonies from nutrient agar plates suspended into TSB and adjusted to 0.5 McFarland standard and fungal spore suspension at

concentration 1×10^6 was prepared. From this inoculum suspension, 10 μl was then added to every well followed by addition of the suitable broth to a final volume of 200 μl in each well. The TSB and SDB, containing DMSO without any tested compound, inoculated with the tested bacterial or fungal suspension, respectively were included as a positive control while the negative control containing TSB or SDB, DMSO, and St/Ag-Se NC without bacterial or fungal suspension was included. Following incubation 37 °C for 24 h for bacteria or at 28 °C for 48 h for filamentous fungi, 50 μl of MTT (0.2 mg/ml) was added followed by incubation at 37 °C for 30 min. The lowest concentration of the tested compound, in the well showed no color change from yellow to pink, was scored as the MIC [42, 43]. The suspension from the MIC containing well and other wells containing the higher concentrations of the tested compound were subcultured on MHA or SDA plates for determination of MBC or MFC, respectively. On completion of incubation, the lowest concentration of the tested compound causing no growth was considered as the MBC for bacteria and MFC for fungi. Subsequently, each microbial strain tolerance level was calculated according to the equation described by [44]:

$$\text{Tolerance level} = \frac{\text{MBC}}{\text{MIC}}$$

The tolerance values of the tested nanocomposite ≤ 2 indicated their bactericidal mode of action with consequent complete microbial cells eradication abilities. Conversely, tolerance values ≥ 4 referred to their bacteriostatic activity with subsequent ability for only bacterial growth inhibition [45].

Biofilm destructive assay

The crystal violet method in microtiter plates was used to evaluate the effect of the biosynthesized St/Ag-Se NC at (1, 0.5, 0.25, 0.125, and 0.0625 mg/ml), against the biofilm forming clinical isolates of *S. aureus, B. subtili, S. epidermidis, E. coli, P. mirabilis, P. aeruginosa, K. pneumonia, S. typhi, A. niger, A. fumigatus, C. albicans,* and *C. herbarum* in 96 well microtitre plate. Each well was inoculated with 180 μl of Luria-Bertani (LB) broth and 10 μl of either bacterial suspension of 0.5 McFarland or 1×10^6 spore/ml of each fungal spore suspension. Ten milliliters of the tested St/Ag-Se NC concentration suspended in DMSO was then added to each well. The plates were incubated at 37 °C for 16 h in case of bacteria or 35 °C for 24 h for fungi and cultures without any tested compound were taken as control. The broth containing suspended cells were gently discarded, wells washed 4 times with 10 μl PBS (pH=7). To each well, 200 μl of 0.4% crystal violet was added followed by incubation for 20 min at 37 °C. The wells washed 3 times with PBS to rinse off the excess crystal violet while, the stain retained by the biofilm was solubilized in 200 μl of 33% acetic acid and incubated for 30 min. The OD, caused by bacterial or fungal biofilm, was measured at 590 nm using an ELISA microtitre plate reader (Multiskan Ascent, Labsystems, Helsinki, Finland). The percentage of biofilm change was calculated according to Hwang et al. [46] using the equation:

$$\textbf{Biofilm change (\%)} = 1 - \frac{\textbf{OD 590 of cells treated with nanocomposite}}{\textbf{OD 590 of untreated cell}} \times 100$$
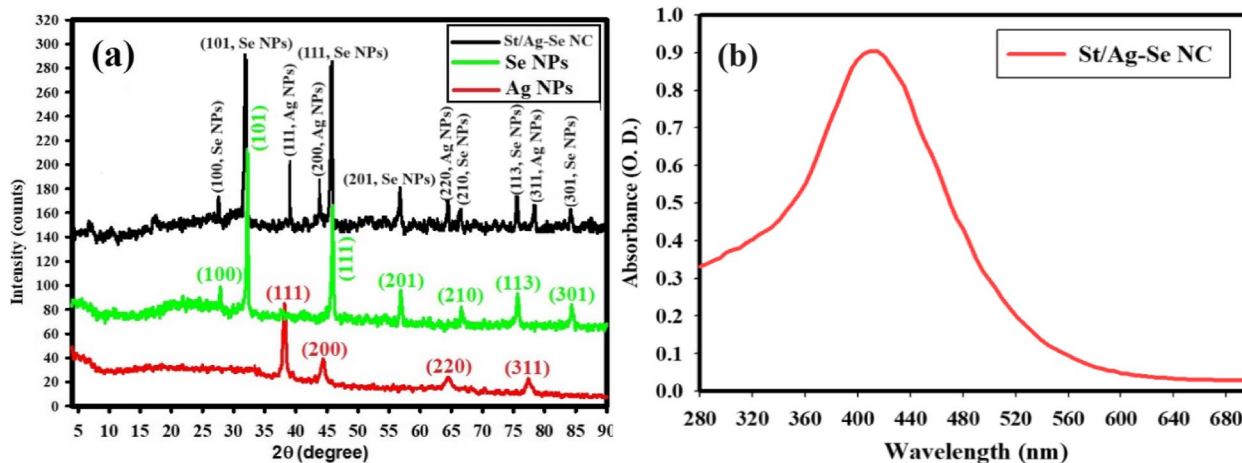

Fig. 1 Crystallinity and optical property of the biosynthesized St/Ag-Se NC, where (**a**) XRD analysis and (**b**) UV-Vis. spectroscopy

Elkady *et al. BMC Microbiology*   (2024) 24:78

Page 6 of 17

Statistical analysis

In the current work, the IC$_{50}$ values were calculated using Graph Pad Prism version 8.01, 2015 (GraphPad software, San Diego, USA) through generating dose response curve by plotting the log concentration versus corresponding viability percentage. In addition, calculation of percentages, mean, standard deviation (SD), and *P*-value values was conducted using Microsoft Excel® ver. 2016.

Results

Characterization of St/Ag-Se NC

XRD analysis and UV-Vis. Spectroscopy

Figure 1a displays the XRD pattern of the biosynthesized St/Ag-Se NC, together with the patterns of Ag NPs and Se NPs for comparison. The pattern clearly indicates the absence of distinct peaks for the first precursors, namely silver nitrate or sodium selenite. The XRD analysis verified the presence of a nano-complex composed of silver-selenium (Ag-Se) and starch (St). Figure 1a displays XRD peaks of Ag NPs, specifically at 2θ angles of 38.88°, 43.09°, 65.90°, and 77.31°. These peaks correspond to the (111), (200), (220), and (311) Bragg's reflections, respectively, and are in agreement with the JCPDS-ICDD 04-0783 card from the Joint Committee on Powder Diffraction Standards (JCPDS). Figure 1a presents the XRD diffraction peaks of Se NPs, indicating the diffraction features at specific angles (2 θ) of 27.78°, 33.10°, 46.67°, 57.98°, 67.10°, 75.66°, and 84.94°. These angles correspond to the Bragg's reflections at (100), (101), (111), (201), (210), (113), and (301) crystal planes, respectively. The peaks exhibited a resemblance to the JCPDS of Se NPs, specifically matching the standard card JCPDS File No 06-0362. Furthermore, the XRD results for all the generated St/Ag-Se NCs exhibit diffraction features at 2θ that are similar to those observed for both Ag NPs and Se NPs. This suggests

that the produced St/Ag-Se NCs possessed a crystalline structure.

The deep brown color observed in the generated substance can be attributed to the activation of the surface Plasmon resonance of biogenic St/Ag-Se NC, providing a reliable spectroscopic signal of their existence. The experimental peak in the spectra (Fig. 1b) was clearly observed as a result of the O.D. (0.906; diluted three times). The UV-Vis analysis revealed that the produced St/Ag-Se NC were minuscule and detectable at a wavelength of 410.0 nm.

DLS analysis and Zeta potential

DLS analysis was performed to determine the particle size distribution in order to evaluate the distribution of particle sizes and calculate the mean size of particles for St/Ag-Se NC. Figure 2a illustrates the results, which are 190.89 nm. The Zeta potential of the produced St/Ag-Se NC was examined at the pH of the synthesis (7.2), as depicted in Fig. 2b. According to the current work, the biosynthesized St/Ag-Se NC maintains a negative surface Zeta potential at the studied pH of the synthesis. Furthermore, due to the negative charge of starch, the Zeta potential of the preparation at a neutral pH of 7.2 was measured to be -41.9 mV, as shown in Fig. 2b.

SEM analysis

Fig. 3 depicts the appearance, shape, and morphological characteristics of the biosynthesized St/Ag-Se NC. Figure 3a shows that bimetallic Ag-Se NPs, which appeared as brilliant particles, were evenly spread throughout starch polymer. According to Fig. (3b), Ag and Se NPs were dispersed uniformly throughout the starch as a clear spherical NPs crowded across the starch polymer.
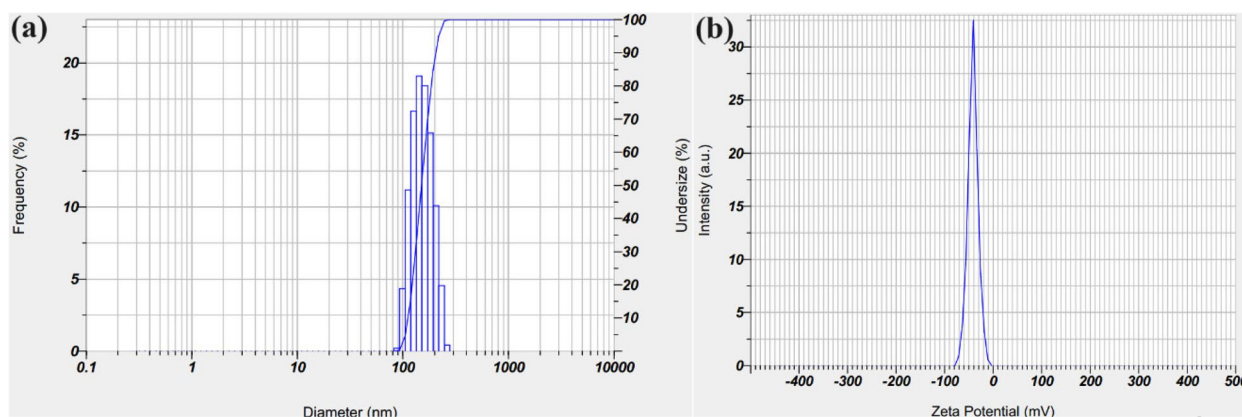

Fig. 2 Particle size distribution and surface charge determination of the biosynthesized St/Ag-Se NC, where (**a**) DLS analysis, and (**b**) Zeta potential
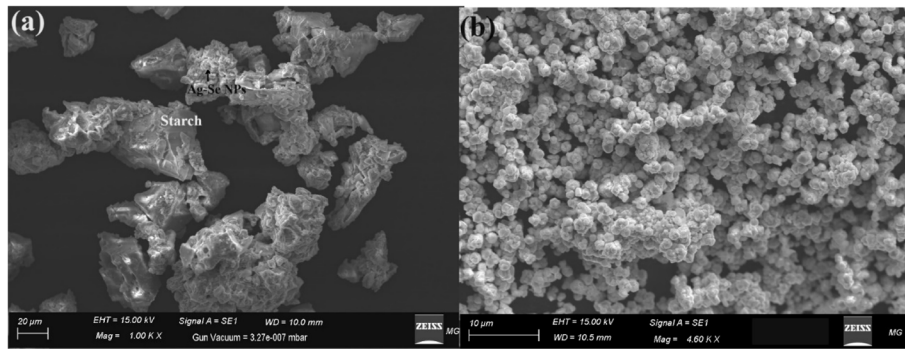
Fig. 3 Morphological surface determination, where (**a**) SEM imaging of the prepared St/Ag-Se NC, and (**b**) SEM imaging of the biosynthesized St/Ag-Se NC at a high magnification
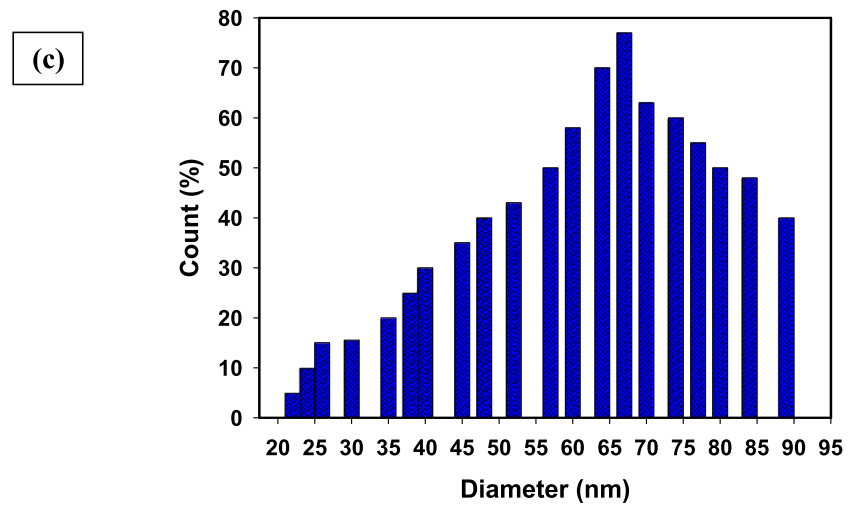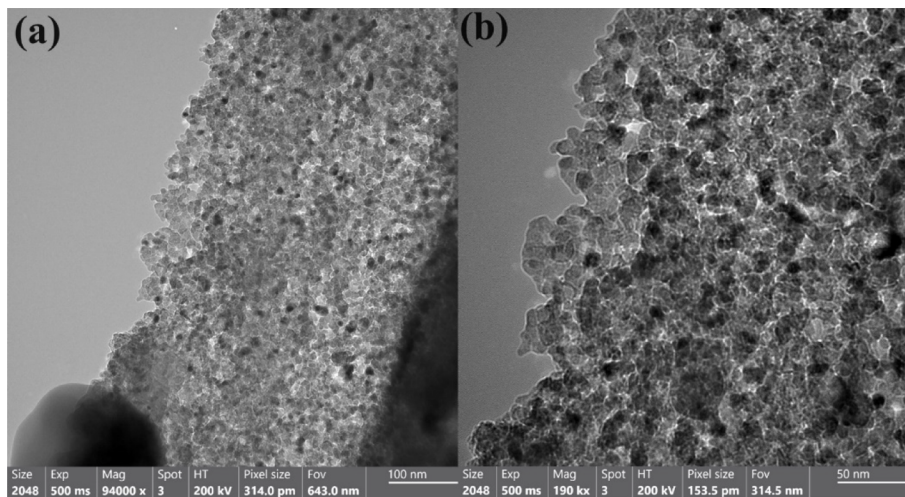

Fig. 4 Mean particle size, and shape, of the biosynthesized St/Ag-Se NC, where (**a**) HR-TEM imaging of the biosynthesized St/Ag-Se NC, (**b**) at a high magnification and (**c**) the histogram of the particle size distribution of the biosynthesized St/Ag-Se NC

HR-TEM analysis

HR-TEM analysis was used for characterization of shape and size of the biosynthesized St/Ag-Se NC (Fig. 4). It was possible to determine the mean size of the particles and see how the biosynthesized St/Ag-Se NC appeared. Additionally, data from HR-TEM and DLS measurements were compared. The produced St/Ag-Se NC have a variety of forms, including oval and spherical morphologies, as seen in HR-TEM Fig. 4a. The biosynthesized St/Ag-Se NC varied in size from 22.6 to 89.45 nm, with a mean diameter of 67.87 nm, as shown in Fig. 4b. The solid lines in Fig. 4c represent the size distribution histogram of the biosynthesized St/Ag-Se NC and confirms the size distribution of the biosynthesized St/Ag-Se NC.

Anti-proliferative activity of Ag St/Ag-Se NC

Exposure of the malignant colon cell line HCT-116 and breast cancer cell line MCF-7 to different concentrations of St/Ag-Se NC, at a range of 0.1 µg/ml–1 mg/ml, illustrated their anti-proliferative outcome. The viability percentages of both cell lines were decreased with the increased concentrations of St/Ag-Se NC, reaching the least value at 1 mg/ml, in comparison with doxorubicin and imatinib that were used as a controls in case
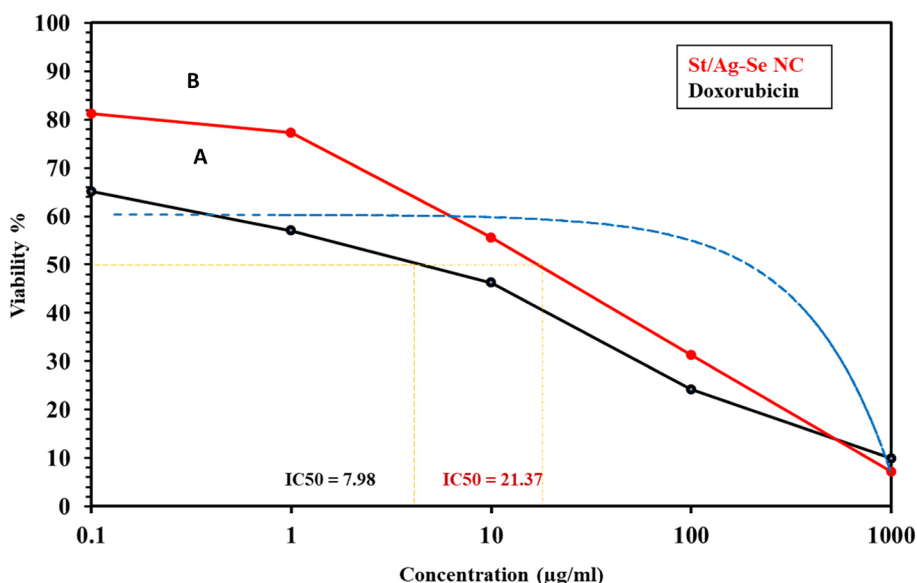

Fig. 5 Anti-proliferative activity of doxorubicin (**A**) and St/Ag-Se NC (**B**) against HCT-116 cell line
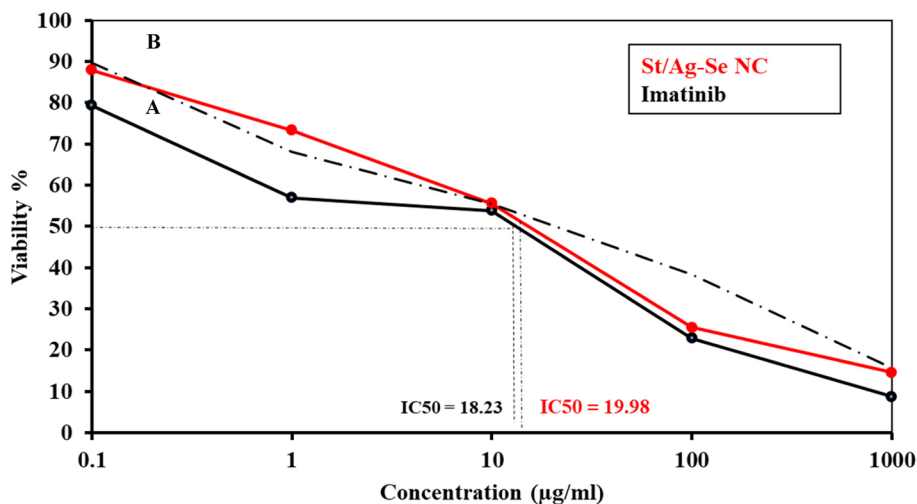

Fig. 6 Anti-proliferative activity of imatinib (**A**) and St/Ag-Se NC (**B**) against MCF-7 cell line
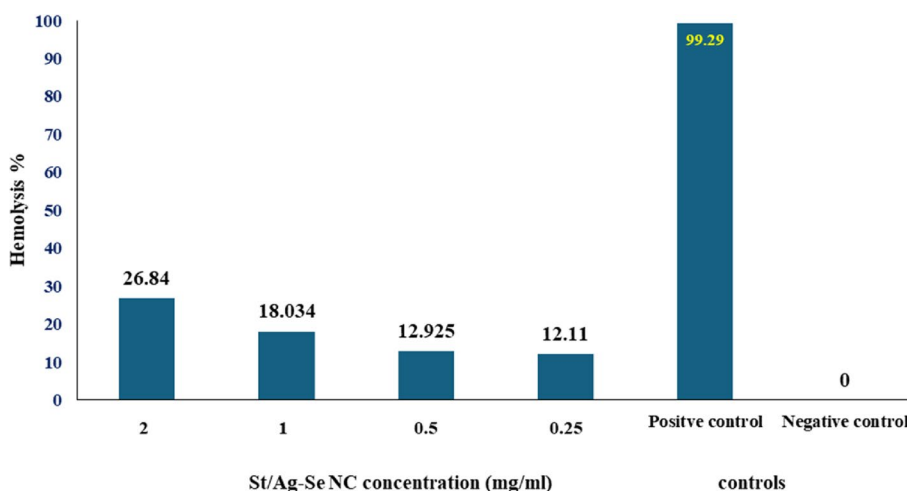
Fig. 7 Hemolytic activity of St/Ag-Se NC at different concentrations in comparison to the positive control (triton X-100) and negative control (PBS)

of HCT-116 and MCF-7 cell lines, respectively. Moreover, the IC_{50} was markedly higher with St/Ag-Se NC than doxorubicin against HCT-116 cell line, with values 21.37 and 7.98 µg/ml, respectively (Fig. 5). While, the IC_{50} was slightly higher with St/Ag-Se NC than imatinib against MCF-7 cell line, with values of 19.98 and 18.23 µg/ml, respectively (Fig. 6).

Blood toxicity of St/Ag-Se NC

Study of St/Ag-Se NC hemolytic activity revealed decreased degree of hemolysis as the nanocomposite concentration decrease. A low hemolysis percentage was recorded at nanocomposite concentration of 0.25 mg/ml in comparison to triton X-100 and PBS (Fig. 7).

Antioxidant activity of St/Ag-Se NC

The results confirmed the increased H_2O_2 scavenging activity of the biosynthesized St/Ag-Se NC with the increased concentration, as compared with ascorbic acid (50 µg/ml) that served as positive control. The highest scavenging activity (42.84%) was observed at a
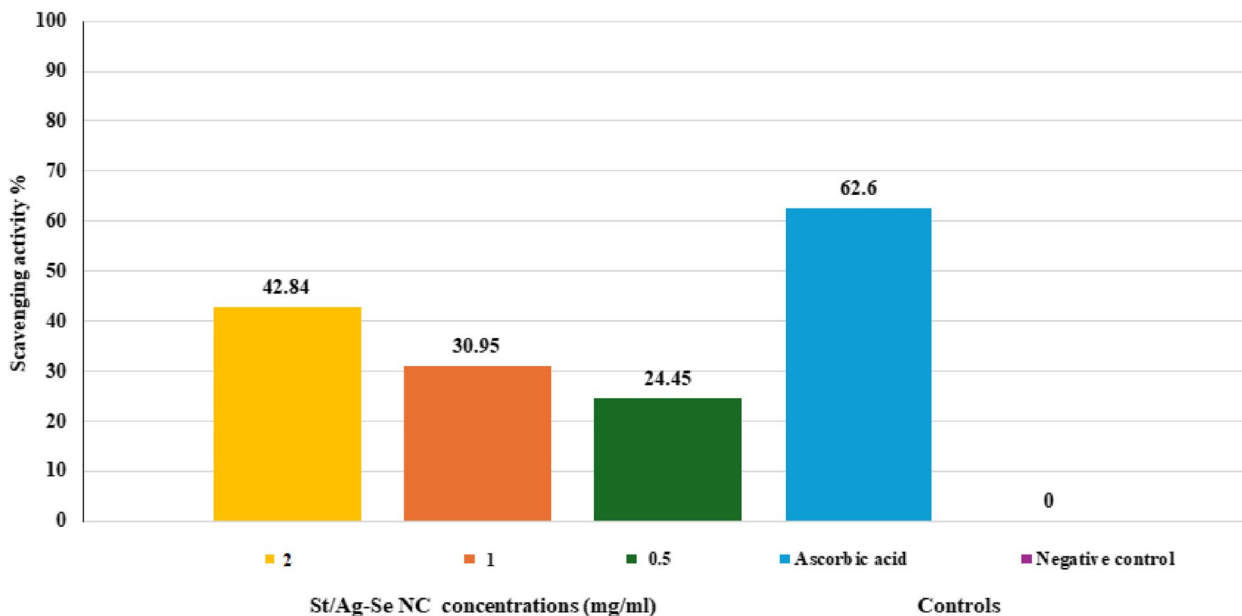

Fig. 8 H_2O_2 scavenging activity of biosynthesized St/Ag-Se NC at different concentrations in comparison to positive control (ascorbic acid) and negative control (PBS)
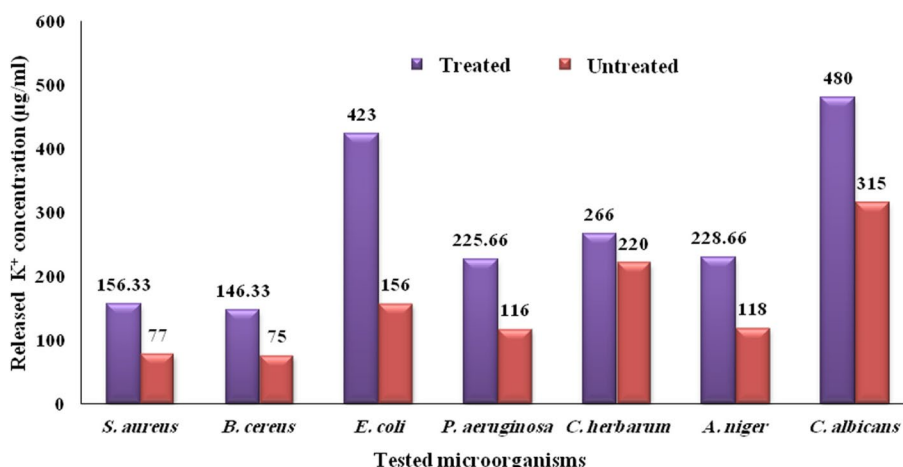
Elkady *et al. BMC Microbiology* (2024) 24:78

Page 10 of 17

Fig. 9 Amount of K **+** released from St/Ag-Se NC treated and untreated microbial cells

concentration of 2 mg/ml St/Ag-Se NC in comparison to 62.5% recorded by ascorbic acid (Fig. 8).

Biosynthesized St/Ag-Se NC potassium leakage effect
The potassium leakage assay was clarify the effect of biosynthesized St/Ag-Se NC, at concentration of 2 mg/ml, on microbial cell membrane. The highest concentration of potassium was detected with *E. coli* and *C. albicans*. This observation may prove, with other results showed in (Fig. 9), the highest impact of St/Ag-Se NC on both bacterial and fungal cells membrane. Statistical analysis of our observations showed significant difference between treated and untreated samples with *P* value 0.021.

Antimicrobial activity of St/Ag-Se NC
Agar well diffusion assay
In the present study, St/Ag-Se NC at a concentration of 2 mg/ml showed antimicrobial activity against most of

the tested bacterial and fungal standard strains including *S. aureus*, *S. epidermidis*, *B. subtilus*, *E. coli*, *P. aeruginosa*, *K. pneumonia*, *P. mirabilis*, A. *niger*, *A. fumigatus*, *C. albicans*, and *C. tropicalis*. Unfortunately, *S. typhi* and *C. herbarum* not affected by the nanocomposite at the applied concentration. Moreover, the highest antibacterial activity was observed against *S. aureus, E. coli*, and *S. epidermidis* with IZDs of 21, 21, and 19 mm, respectively in comparison to chloramphenicol (30 μg/ml) that displayed IZDs 28, 24, and 24 mm, respectively. On the other hand, the maximum antifungal activity was observed against *C. albicans* and showed IZD 28 mm, in comparison to fluconazole (50 μg/ml) with IZD 32 mm (Figs. 10 and 11).

Inhibitory concentrations of St/Ag-Se NC
The highest antibacterial activity of St/Ag-Se NC was observed against *S. epidermidis* with lowest MIC (18.75
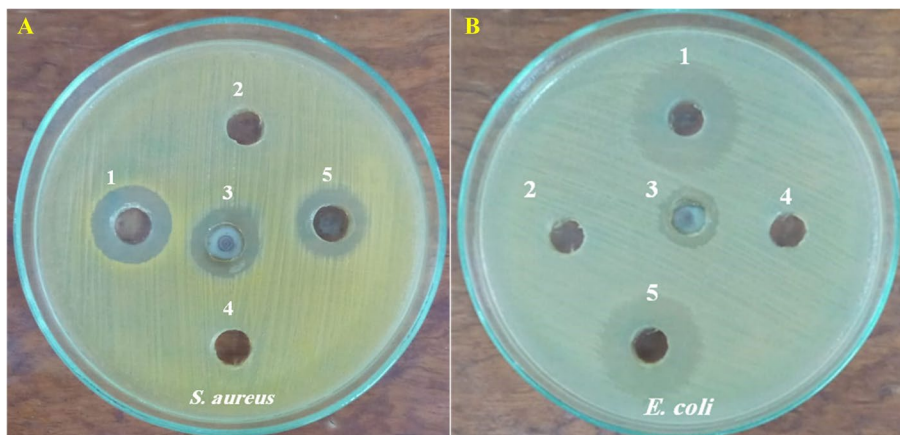

Fig. 10 Antimicrobial activity of St/Ag-Se NC using agar well diffusion method against S. aureus ATCC 6538 (**A**) and E. coli ATCC 8739 (**B**). Wells 1; Tested St/Ag-Se Nc, 2; Sodium selenite, 3; AgNO$_3$, 4; Starch, and 5; Positive control, chloramphenicol
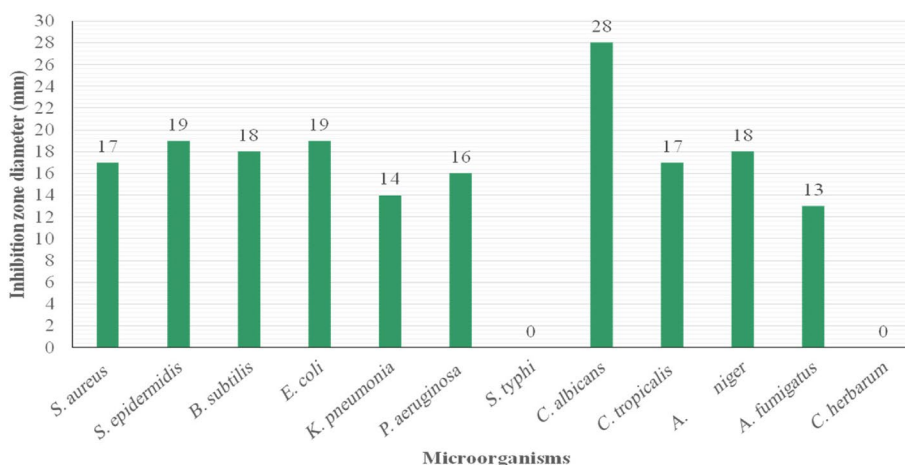
Fig. 11 Various IZDs caused by St/Ag-Se NC, in agar well diffusion assay, against the tested microbial strains
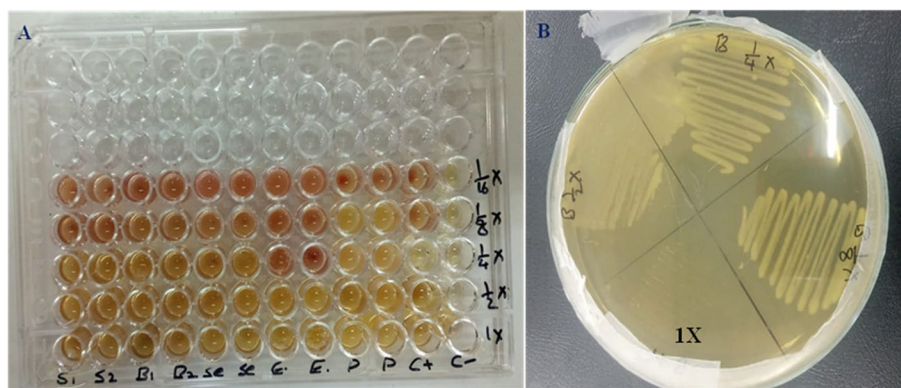

Fig. 12 Representative St/Ag-Se NC antimicrobial activity. **A** Broth microdilution assay. Wells S; S. aureus ATCC 6538, B; B. subtilis ATCC 6633, Se; S. epidermidis ATCC 12,228, E; E. coli ATCC 8739, P. aeruginosa ATCC 9027, C+; Positive control; C-; Negative control, and 1X-1/16X; Serial dilutions. **B** Minimum bactericidal concentration assay. 1X dilution showed no growth and recorded as MBC

µg/ml) followed by *S. aureus, E. coli*, and *B. subtilis* with MIC of 25 µg/ml for each. On the other hand, the maximum antifungal activity was observed against *C. albicans* where the MIC was 50 µg/ml. In addition, the MBC was observed with nanocomposite concentration of 25 µg/ml against *S. aureus, B. subtilis*, and *E. coli*. Similarly, the MFC was noticed as 100 µg/ml against all of the tested fungi while, the microbial tolerance was unity with *S. aureus, B. subtilis, E. coli, C. tropicalis*, and *A. fumigatus* (Fig. 12 and Table 1).

Anti-biofilm activity of St/Ag-Se NC

The effect of St/Ag-Se NC, at different concentrations, on various bacterial and fungal biofilm was noticeable. High biofilm changes, at concentration 1 mg/ml, were observed with *S. epidermidis* and *B. subtilis* at 87.5% and 82.5%, respectively. In addition, *S. aureus, E. coli*, and *P. mirabilis* showed high changes in their biofilms, 68.05%,

66.12%, and 65.37%, respectively, when treated with 0.5 mg/ml of St/Ag-Se NC (Table 2).

Discussion

Nanocomposite material contains number of phases with at least one dimension of which in nanometer scale. These dimension enhance materials characters as it creates a very vital phase interfaces [47, 48]. The usual availability, best antimicrobial activities, and low human cytotoxicity of Ag NPs reflect their extensive applications in biomedical field [49, 50]. Additionally, selenium is one of the micronutrients essential for human's healthy body with anti-inflammatory and redox activities. It is essential for activation of human's immunity and nervous system. As well, cardiomyopathies and other several diseases has been alleviated with proper selenium supplements [51].

The intensity of the deep brown color corresponded to the capacity to biosynthesize St/Ag-Se NC. The physical

Table 1 The MICs, MBCs, and MFCs of St/Ag-Se NC and their tolerance by various microbial isolates

Tested Microorganism	Antimicrobial activity			Tolerance
	MIC[a]	MBC	MFC	
	µg/ml			
S. aureus ATCC 6538	25	25	-	1
S. epidermidis ATCC 12,228	18.75	50	-	2.67
B. subtilis ATCC 6633	25	25	-	1
E. coli ATCC 8739	25	25	-	1
K. pneumonia ATCC 13,882	75	200	-	2.67
P. aeruginosa ATCC 9027	75	100	-	1.33
P. mirabilis ATCC25933	100	200	-	2
C. albicans ATCC 10,231	50	-	100	2
C. tropicalis ATCC 13,803	100	-	100	1
A. niger CBS 31.29	75	-	100	1.33
A. fumigatus CBS 106	100	-	100	1

[a] *MIC* Minimum inhibitory concentration, *MBC* Minimum bactericidal concentration, and *MFC* Minimum fungicidal concentration

Table 2 Microbial biofilm suppression (%) by different concentrations of St/Ag-Se NC

Tested microorganisms	Biofilm change (%)/St/Ag-Se NC concentration (mg/ml)				
	1	0.5	0.25	0.125	0.0625
S. aureus	77.37	68.05	49.94	19.59	16.38
B. subtilis	82.68	55.37	38.43	16.07	4.945
S. epidermidis	87.55	73.44	36.34	16.94	12.14
E. coli	77.78	66.12	54.16	26.24	7.737
P. mirabilis	73.08	65.37	52.17	18.27	4.662
P. aeruginosa	70.48	59.55	48.83	15.85	10.35
K. pneumonia	76.19	57.16	47.35	18.78	6.502
S. typhi	27.53	19.84	18.07	14.51	6.307
A. niger	31.98	27.97	24.14	21.28	12.05
A. fumigatus	27.45	22.12	13.16	11.96	4.57
C. albicans	77.76	63.35	32.67	25.13	13.97
C. herbarum	76.04	61.15	59.44	30.71	7.07

characteristics, such as strength, size, surface structure, and dielectric properties, of NPs play a crucial role in surface plasmon resonance (SPR). It is worth mentioning that a little 2θ shift was observed, which may be attributed to the formation of St/Ag-Se NC. The lack of peaks at 2θ = 31.30°, 32.62°, and 33.68° suggests that the synthesized Ag NPs, Se NPs, and Ag-Se NPs were pure and did not contain any AgO NPs or SeO NPs [52–54]. Furthermore, the XRD results demonstrate that the synthesized possess a high degree of crystallinity, which enhances their suitability for various applications [41].

The produced St/Ag-Se NC, in the present study, were uniformly distributed with wide size and the same spherical shape, according to a comparison of the literature about the morphological shape and analysis of elements. Bimetallic silver and gold core-shell NPs were created by [55] using the citrate reduction process at various pH levels and temperatures. The acquired morphological form and boundary size suggested that they had a size varied from 50 to 65 nm and seem as spherical particles, which means that both pH and temperature play a crucial role in the creation process. Finally, our findings were compared with the newly published studies [56–59].

As well, the produced St/Ag-Se NC varied in size and were mostly spherical in form, according to a comparison of average particle size and shape in the literature. Castro-Longoria et al. [60] mycosynthesized silver, gold, and silver-gold bimetallic NPs, where the shape of the NPs was found to be mainly spherical with a mean diameter of 11.0 nm for silver and 32.0 nm for gold.

Although different morphologies may be noticed owing to the synthetic process from extract, the anisotropic shape had been recorded, the created forms in that work [60], may be varied as the shape of extracted NPs was roughly circular or ellipsoidal in all cases. Due to the use of only one reducing and capping agent, a constant form is seen in our investigation. Finally, our findings were compared with the newly published studies [61–64].

It is important to note that the starch used, which served as a suitable capping and stabilizing agent, was responsible for the creation of the mono-distributed NPs [65]. Dynamic light scattering analysis determines the hydrodynamic diameter of NPs surrounded by water molecules, which leads to larger sizes of the capped NPs. On the other hand, HR-TEM analysis calculates the actual particle size of the substance without the solvent layer. Consequently, it is typical for DLS size measurements to exhibit higher values compared to HR-TEM measurements [66]. The NPs that were produced were highly dispersed in a restricted range of sizes due to the scientific validity of DLS, which significantly improved their characteristics and applications [67–70].

Upon comparing our combination St/Ag-Se NC with existing literature on particles of intermediate size and form, we discovered that our particles were poly-dispersed, exhibited size variation, and predominantly had spheroidal shapes. Diverse forms may have been developed in that work. While the majority of the newly biosynthesized St/Ag-Se NCs exhibited spherical or oval shapes, variations in morphology were observed due to the extraction-based synthetic procedure, leading to the detection of anisotropic forms. Poly-dispersed NPs are

Elkady *et al. BMC Microbiology*   (2024) 24:78

Page 13 of 17

the stable form achieved in our work, as we exclusively employed the most practicable reducing and capping agent, starch.

Biomedical applications of nanocomposites critically depend on their cytotoxic effect on different human cells [17, 71]. In the current study, a clear low anti-proliferative outcomes of different biosynthesized St/Ag-Se NC concentrations against two malignant cell lines were reported. The least viability percentages of both cell lines were observed when exposed to the nanocomposite at 1 mg/ml. A higher value of IC_{50} (21.37 µg/ml) of St/Ag-Se NC against malignant colon cell line HCT-116, in comparing with doxorubicin IC_{50} (7.98 µg/ml), was obtained which reflect slightly low toxic activity. While, a little higher IC_{50} (19.98 µg/ml) than imatinib (18.32 µg/ml) was recorded against breast cancer cell line MCF-7. In a relatively related study, Abdallah et al. [72] recorded about 1.118 and 0.119 mg/ml as an IC_{50} for biosynthesized polyvinyl alcohol/silver (PVA/Ag) and chitosan/silver (CS/Ag) nanocomposites, respectively, against Huh-7 cell line. On the same way of our results, [73] and [74] revealed chitosan nanocomposite with LC_{50} of 0.125 mg/ml and 0.518 mg/ml against HeLa cell lines and brine shrimp, respectively. These high IC_{50} values indicated the high biosafety of the biogenic nanocomposites against the tested cell lines.

Interestingly, the low absorbance, which represents the lowest level of hemolysis, was observed at a concentration of 0.25 mg/ml of St/Ag-Se NCs. Our observations were in the same context with the study conducted by Jayeoye et al. [75] who reported an increased hemolysis percentage as the poly (vinyl alcohol-co-ethylene glycol)/poly (3-aminophenyl boronic acid) nanocomposite concentration increase. Similarly, the polypyrrole nanocomposites concentration below 2.5 mg/ml exhibited hemolysis level lower than 5% [76]. These results indicates the great influence of nanocomposites hemolytic activity by their concentration and particularly high concentration had the most significant impact on RBCs destruction compared to other tested concentrations. The enhanced nanocomposites haemocompatibility may be associated with the biocompatible character of starch, poly (vinyl alcohol-co-ethylene glycol)/poly (3-aminophenyl boronic acid) and polypyrrole. Moreover, the nanocomposites erythrocytes toxicity could be correlated to pits development on RBCs membrane with subsequent pores formation and osmotic rupture.

Our findings provided confirmation of the enhanced H_2O_2 scavenging activity exhibited by the biosynthesized St/Ag-Se NC. As the concentration of the nanocomposite increased, its H_2O_2 scavenging activity increased. When compared to the positive control, ascorbic acid (50 µg/ml), the St/Ag-Se NC (2 mg/ml) demonstrated high scavenging activity (42.84%). A related results were obtained by Hasanin et al. [43] study which recognized forceful antioxidant effect of mycosynthesized starch/copper nanocomposite, at different concentrations, with relatively equal activity to ascorbic acid. In the same context, high H_2O_2 scavenging percentage by Ag NPs was spectrophotometrically observed by M et al. [77] study, in comparing with ascorbic acid. At 0.1 mg/ml of Ag NPs, significant H_2O_2 scavenging activity (86.47%) was found. These results impressively suggest the utilization of biosynthesized nanocomposites as antioxidant agents for controlling of various degenerative disorders caused by reactive oxygen species.

In our research, the cytoplasmic potassium leakage assay illustrate the effect of biosynthesized St/Ag-Se NC on both bacterial and fungal cells membrane. In a related study, the amount of cellular protein released from bacterial cells was directly proportional to the applied nanocomposites concentration [78]. These findings clarify the cell membrane dysfunction activity of St/Ag-Se NC as a possible mechanism of nanocomposites microbial cells killing effect.

In the present study, agar well diffusion assay showed the good antimicrobial activity of St/Ag-Se NC (2 mg/ml) against all the tested microbial standard strains except *S. typhi* and *C. herbarum*. *Staph aureus, E. coli*, and *S. epidermidis* were highly affected with IZDs of 21, 21, and 19 mm, respectively in comparing with chloramphenicol (30 µg/ml) that showed IZDs 28, 24, and 24 mm, respectively. On the other hand, *C. albicans* was vastly affected with IZD 28 mm, in comparing with 32 mm IZD demonstrated with fluconazole (50 µg/ml). Our results were highly compatible with Abdallah et al. [72] who biosynthesized PVA/Ag and CS/Ag nanocomposites with clear effect on MDR bacteria. The PVA/Ag and CS/Ag nanocomposites showed significant antimicrobial activities against both Gram-positive and Gram-negative bacteria with IZDs ranging between 33 ± 3 and 21 ± 1 mm for PVA/Ag and 14 ± 2 and 8 ± 0.5 mm in case of CS/Ag. As well, their maximum activity demonstrated against *S. epidermidis* while, minimum activity was noticed against *K. pneumonia* and *S. aureus*. These inhibitory effects could be clarify the enhanced diffusion and incessant release of metal NPs from the biosynthesized nanocomposites into the nearby agar medium and subsequently large IZDs. Also, the broad range of the biosynthesized St/Ag-Se NC activity against the majority of the tested bacterial and fungal strains indicate their advantage as a non-specific antimicrobial agent.

In our study, *S. epidermidis* was the uppermost affected bacterial strains with St/Ag-Se NC MIC of 18.75 µg/ml. Also, *B. subtilis*, *S. aureus*, and *E. coli* were highly affected with equal MIC and MBC (25 µg/ml) for all strains. As

well, the highest fungal destructive effect was demonstrated against *C. albicans* with MIC of 50 µg/ml. On top, *S. aureus*, *B. subtilis*, *E. coli*, *P. mirabilis*, *C. tropicalis*, and *(A) fumigatus* showed microbial tolerance ≤ 2. In related studies, lower MIC (15 µg/ml) of selenium/silver nanocomposite against *(B) subtilis* and *E. coli* was reported [79]. While, Abd-Elraoof et al. [80] quantitatively assessed chitosan/selenium nanocomposite activity against *S. typhimurium*, *S. aureus*, and *E. coli* revealing MIC of 17.5, 20, and 25 µg/ml, respectively. Additionally, our results were consistent with Amr et al. [45] findings that demonstrated biosynthesized Ag NPs with an equal MICs and MBCs (1000 µg/ml) against *P. aeruginosa*, *E. coli*, and *K. quasipneumoniae* and subsequent MBC/MIC ratio equal one. Similarly, *E. coli*, *K. pneumoniae*, *P. aeruginosa*, *Salmonella enterica*, and *Salmonella infantis* showed biogenic Ag NPs MBC/MIC ratio ≤ 2 [81]. The fungal level, selenium/chitosan nanocomposite showed activity against *(C) albicans* with low MICs of 25 µg/ml [42]. As well, Arsène et al. [82] use *Aloe vera* extract for Ag NPs synthesis with high activity against four *Candida albicans* strains where the MICs range 16–32 µg/ml. While, Chatterjee et al. [83] silver NPs prevented the tested *Aspergillus* spp. observable growth (MIC) at 8–128 µg/ml and exhibited fungicidal effect at 32–256 µg/ml. The variability of the obtained MIC values might be reflect the reducing agents variation in different biogenic method with consequential inconsistence NPs shape, size, and stabilizing agents [84–86]. Also, significant dissimilarity in microbial cells wall composition might be attributed to uneven MIC. The results also indicate the acceptable activity with low microbial tolerability of the tested strains to the biosynthesized St/Ag-Se NC and their activity as germicidal agent against the majority of tested strains. The ultrafine St/Ag-Se NC (22.6-89.45 nm) could be reflect their high efficacy at little concentration.

In the current study, the impact of different concentrations of St/Ag-Se NC on various bacterial and fungal biofilms was evident. Significant alterations in biofilm formation were observed at a concentration of 1 mg/ml. A substantial decrease of 87.5% and 82.5% in biofilm formation for *S. epidermidis* and *B. subtilis*, respectively were recorded. Furthermore, *S. aureus*, *E. coli*, and *P. mirabilis* exhibited notable reductions in biofilm formation of 68.05%, 66.12%, and 65.37%, respectively when treated with 0.5 mg/ml of St/Ag-Se NC. Our findings were consistent with Bellisario et al. [87] who recorded variable silver/polypropylene nanocomposites antibiofilm activity against *K. pneumoniae* and *S. aureus*. Additionally, El-Behery et al. [88] reported poor biofilm formation by *S. aureus*, *E. coli*, and *C. albicans* (90.62%, 90.70%, and 90.88%, respectively) after treatment with silver/selenium nanocomposite. The collected results illustrate the increased activity of bimetalic combination as well as, the proportional correlation between the nanocomposites concentration and their biofilm inhibitory effect that could be recommend their future relevance as one of the preventive measures for microbial biofilm formation.

Conclusion

In the current study, a nanocomposite based on starch, silver and selenium was biosynthesized using ecofriendly method. The whole characters of biosynthesized St/Ag-Se Nc were determined following the UV-Vis, XRD, DLS, Zeta potential, SEM, and HR-TEM analysis. The obtained nanocomposite was pure, crystalline, oval and spherical in shape, with a mean particle diameter of 67.87 nm. The nanocomposite displayed promising antimicrobial activities against wide range of bacterial and fungal species which suggest its feasible using as an alternative broad spectrum antimicrobial agents. Their effective microbial biofilm suppression as well as, low cytotoxic and hemolytic activities indicated their possible application in biomedical intentions.

Availability of data and materials
No datasets were generated or analysed during the current study.

Declarations

Ethics approval and consent to participate
Not applicable.

Consent for publication
Not applicable.

Competing interests
The authors declare no competing interests.

Author details
[1]Microbiology and Immunology Department, Faculty of Pharmacy (Boys), Al-Azhar University, Cairo 11884, Egypt. [2]Botany and Microbiology Department, Faculty of Science, Al-Azhar University, Cairo 11884, Egypt. [3]Department of Microbiology and Immunology, Faculty of Pharmacy, Ahram Canadian (ACU), Giza, Egypt. [4]Department of Microbiology and Immunology, Faculty of Pharmacy, Galala University, New Galala City, Suez, Egypt. [5]Drug

Elkady *et al. BMC Microbiology*   (2024) 24:78

Page 15 of 17

Microbiology Lab., Drug Radiation Research Department, National Center for Radiation Research and Technology (NCRRT), Egyptian Atomic Energy Authority (EAEA), Cairo, Egypt. [6]Department of Microbiology and Immunology, Faculty of Medicine, Al-Azhar University, Cairo 11884, Egypt.

References

1. Prestinaci F, Pezzotti P, Pantosti A. Antimicrobial resistance: a global multifaceted phenomenon. Pathogens Global Health. 2015;109(7):309–18. https://doi.org/10.1179/2047773215Y.0000000030.

2. Colson AR, Morton A, Årdal C, Chalkidou K, Davies SC, Garrison LP, Jit M, Laxminarayan R, Megiddo I, Morel C, Nonvignon J, Outterson K, Rex JH, Sarker AR, Sculpher M, Woods B, Xiao Y. Antimicrobial Resistance: is Health Technology Assessment Part of the solution or part of the Problem? Value Health. 2021;24(12):1828–34. https://doi.org/10.1016/j.jval.2021.06.002.

3. Catalano A, Iacopetta D, Ceramella J, Scumaci D, Giuzio F, Saturnino C, Aquaro S, Rosano C, Sinicropi MS. Multidrug Resistance (MDR): a widespread phenomenon in pharmacological therapies. Molecules. 2022;27(3): 616.

4. Ventola CL. The antibiotic resistance crisis: part 1: causes and threats. Pharm Ther. 2015;40(4):277.

5. Said A, El-Gamal MS, Abu-Elghait M, Salem SS. Isolation, identification and antibiotic susceptibility pattern of urinary tract infection bacterial isolates. Lett Appl Nanobiosci. 2021;10(4):2820–30. https://doi.org/10.33263/LIANBS104.28202830.

6. Ferlay J, Ervik M, Lam F, Colombet M, Mery L, Piñeros M, Znaor A, Soerjomataram I, Bray F. Global cancer observatory: cancer today. Lyon: International agency for research on cancer. 2018;3(20):2019.

7. Schirrmacher V. From chemotherapy to biological therapy: a review of novel concepts to reduce the side effects of systemic cancer treatment. Int J Oncol. 2019;54(2):407–19.

8. Saied E, Salem SS, Al-Askar AA, Elkady FM, Arishi AA, Hashem AH. Mycosynthesis of Hematite (alpha;-Fe2O3) Nanoparticles Using Aspergillus niger and Their Antimicrobial and Photocatalytic Activities. Bioengineering. 2022;9(8):397.

9. Hashem AH, Hasanin M, Kamel S, Dacrory S. A new approach for antimicrobial and antiviral activities of biocompatible nanocomposite based on cellulose, amino acid and graphene oxide. Colloids Surf B. 2022;209: 112172. https://doi.org/10.1016/j.colsurfb.2021.112172.

10. Ali OM, Hasanin MS, Suleiman WB, Helal EE-H, Hashem AH. Green biosynthesis of titanium dioxide quantum dots using watermelon peel waste: antimicrobial, antioxidant, and anticancer activities. Biomass Convers Biorefinery. 2022. https://doi.org/10.1007/s13399-022-02772-y.

11. Hashem AH, Saied E, Amin BH, Alotibi FO, Al-Askar AA, Arishi AA, Elkady FM, Elbahnasawy MA. Antifungal activity of Biosynthesized Silver nanoparticles (AgNPs) against Aspergilli Causing aspergillosis: Ultrastructure Study. J Funct Biomaterials. 2022;13(4):242.

12. Albalawi MA, Abdelaziz AM, Attia MS, Saied E, Elganzory HH, Hashem AH. Mycosynthesis of silica nanoparticles using aspergillus Niger: control of Alternaria Solani Causing Early Blight Disease, induction of Innate Immunity and reducing of oxidative stress in Eggplant. Antioxidants. 2022;11(12): 2323.

13. El-Khawaga AM, Elsayed MA, Gobara M, Soliman AA, Hashem AH, Zaher AA, Mohsen M, Salem SS. Green synthesized ZnO nanoparticles by Saccharomyces cerevisiae and their antibacterial activity and photocatalytic degradation. Biomass Convers Biorefinery. 2023. https://doi.org/10.1007/s13399-023-04827-0.

14. Abdelfattah NAH, Yousef MA, Badawy AA, Salem SS. Influence of biosynthesized magnesium oxide nanoparticles on growth and physiological aspects of cowpea (Vigna unguiculata L.) plant, cowpea beetle, and cytotoxicity. Biotechnol J. 2023;18(12): 2300301. https://doi.org/10.1002/biot.202300301.

15. Hussein AS, Hashem AH, Salem SS. Mitigation of the hyperglycemic effect of streptozotocin-induced diabetes albino rats using biosynthesized copper oxide nanoparticles. Biomol Concepts. 2023;14(1): 20220037. https://doi.org/10.1515/bmc-2022-0037.

16. Salem SS, Hammad EN, Mohamed AA, El-Dougdoug W. A Comprehensive Review of nanomaterials: types, synthesis, characterization, and applications. Biointerface Res Appl Chem. 2023;13(1). https://doi.org/10.33263/BRIAC131.041.

17. Dezfuli AAZ, Abu-Elghait M, Salem SS. Recent insights into Nanotechnology in Colorectal Cancer. Appl Biochem Biotechnol. 2023. https://doi.org/10.1007/s12010-023-04696-3.

18. Yang C, Li W, Yang Z, Gu L, Yu Y. Nanoconfined antimony in sulfur and nitrogen co-doped three-dimensionally (3D) interconnected macroporous carbon for high-performance sodium-ion batteries. Nano Energy. 2015;18:12–9.

19. Abdelmoneim HE, Wassel MA, Elfeky AS, Bendary SH, Awad MA, Salem SS, Mahmoud SA. Multiple Applications of CdS/TiO2 Nanocomposites Synthesized via Microwave-Assisted Sol-Gel. J Clust Sci. 2022;33:1119–28. https://doi.org/10.1007/s10876-021-02041-4.

20. Hashem AH, Selim TA, Alruhaili MH, Selim S, Alkhalifah DHM, Al Jaouni SK, Salem SS. Unveiling Antimicrobial and Insecticidal Activities of Biosynthesized Selenium Nanoparticles Using Prickly Pear Peel Waste. J Funct Biomater. 2022;13(3):112. https://doi.org/10.3390/jfb13030112.

21. Abdelraof M, Ibrahim S, Selim M, Hasanin M. Immobilization of L-methionine γ-lyase on different cellulosic materials and its potential application in green-selective synthesis of volatile sulfur compounds. J Environ Chem Eng. 2020;8(4):103870.

22. Shehabeldine A, El-Hamshary H, Hasanin M, El-Faham A, Al-Sahly M. Enhancing the antifungal activity of griseofulvin by incorporation a green biopolymer-based nanocomposite. Polymers. 2021;13(4): 542.

23. Hasanin MS, El-Sakhawy M, Ahmed HY, Kamel S. Hydroxypropyl methylcellulose/graphene oxide composite as drug carrier system for 5-Fluorouracil. Biotechnol J. 2021;e2100183.

24. Hasanin MS. Simple, economic, ecofriendly method to extract starch nanoparticles from potato peel waste for biological applications. Starch-Stärke. 2021;73:2100055.

25. Dagher S, Haik Y, Ayesh AI, Tit N. Synthesis and optical properties of colloidal CuO nanoparticles. J Lumin. 2014;151:149–54.

26. Al-Johani H, Salam MA. Kinetics and thermodynamic study of aniline adsorption by multi-walled carbon nanotubes from aqueous solution. J Colloid Interface Sci. 2011;360(2):760–7.

27. Sugijanto NE, Diesel A, Ebel R, Indrayanto G, Zaini NC. Chemical constituents of the endophytic fungus Lecythophora sp. isolated from Alyxia reinwardtii. Nat Prod Commun. 2009;4(11):1934578X0900401109.

28. Olawale F, Ariatti M, Singh M. Biogenic Synthesis of Silver-Core Selenium-Shell nanoparticles using Ocimum tenuiflorum L.: response surface methodology-based optimization and Biological Activity. Nanomaterials. 2021;11(10): 2516.

29. Ashour AH, El-Batal AI, Maksoud MIAA, El-Sayyad GS, Labib S, Abdeltwab E, El-Okr MM. Antimicrobial activity of metal-substituted cobalt ferrite nanoparticles synthesized by sol–gel technique. Particuology. 2018;40:141–51. https://doi.org/10.1016/j.partic.2017.12.001.

30. Abdel Maksoud MIA, El-Sayyad GS, Ashour AH, El-Batal AI, Abd-Elmonem MS, Hendawy HAM, Abdel-Khalek EK, Labib S, Abdeltwab E, El-Okr MM. Synthesis and characterization of metals-substituted cobalt ferrite [Mx Co(1-x) Fe2O4; (M = zn, Cu and Mn; x = 0 and 0.5)] nanoparticles as antimicrobial agents and sensors for Anagrelide determination in biological samples. Mater Sci Engineering: C. 2018;92:644–56. https://doi.org/10.1016/j.msec.2018.07.007.

31. Hashem AH, El-Sayyad GS. Antimicrobial and anticancer activities of biosynthesized bimetallic silver-zinc oxide nanoparticles (Ag-ZnO NPs) using pomegranate peel extract. Biomass Convers Biorefinery. 2023:1–13.

32. Hasanien YA, Mosleh MA, Abdel-Razek AS, El-Sayyad GS, El-Hakim EH, Borai EH. Green synthesis of SiO2 nanoparticles from Egyptian white sand using submerged and solid-state culture of fungi. Biomass Convers Biorefinery. 2023:1–14.

33. Elkhodary BH, Attia MS, El-Sayyad GS, Salem MS. Effectiveness of bimetallic ZnO-B2O3 nanoparticles produced by Streptomyces gancidicus as prospective antifungal agents and therapeutic nutrients to enhance pea plant immunity against damping off-causing Pythium irregulare: in vivo and in vitro investigations. Biomass Convers Biorefinery. 2023:1–24. https://doi.org/10.1007/s13399-023-04913-3.

34. Hammad SE, El-Rouby MN, Abdel-Aziz MM, El-Sayyad GS, Elshikh HH. Endophytic fungi–assisted biomass synthesis of gold, and zinc oxide nanoparticles for increasing antibacterial, and anticancer activities.

Elkady *et al. BMC Microbiology*   (2024) 24:78

Page 16 of 17

Biomass Convers Biorefinery. 2023;1–18. https://doi.org/10.1007/s13399-023-04954-8.

35. Fatima N, Khan MM, Khan IA. L-asparaginase produced from soil isolates of Pseudomonas aeruginosa shows potent anti-cancer activity on HeLa cells. Saudi J Biol Sci. 2019;26(6):1146–53. https://doi.org/10.1016/j.sjbs.2019.05.001.

36. Gonçalves JCR, Coulidiati TH, Monteiro AL, de Carvalho-Gonçalves LCT, de Oliveira Valença W, de Oliveira RN, de Amorim Câmara C, de Araújo DAM. Antitumoral activity of novel 1, 4-naphthoquinone derivative involves L-type calcium channel activation in human colorectal cancer cell line. J Appl Biomed. 2016;14(3):229–34.

37. Liaqat N, Jahan N, Khalil Rahman, Anwar T, Qureshi H. Green synthesized silver nanoparticles: optimization, characterization, antimicrobial activity, and cytotoxicity study by hemolysis assay. Front Chem. 2022;10:952006. https://doi.org/10.3389/fchem.2022.952006.

38. Keshari AK, Srivastava R, Singh P, Yadav VB, Nath G. Antioxidant and antibacterial activity of silver nanoparticles synthesized by Cestrum nocturnum. J Ayurveda Integr Med. 2020;11(1):37–44. https://doi.org/10.1016/j.jaim.2017.11.003.

39. Khater MS, Kulkarni GR, Khater SS, Gholap H, Patil R. Study to elucidate effect of titanium dioxide nanoparticles on bacterial membrane potential and membrane permeability. Mater Res Express. 2020;7(3):035005.

40. Balouiri M, Sadiki M, Ibnsouda SK. Methods for in vitro evaluating antimicrobial activity: a review. J Pharm Anal. 2016;6(2):71–9.

41. Elakraa AA, Salem SS, El-Sayyad GS, Attia MS. Cefotaxime incorporated bimetallic silver-selenium nanoparticles: promising antimicrobial synergism, antibiofilm activity, and bacterial membrane leakage reaction mechanism. RSC Adv. 2022;12(41):26603–19. https://doi.org/10.1039/D2RA04717A.

42. Filipović N, Ušjak D, Milenković MT, Zheng K, Liverani L, Boccaccini AR, Stevanović MM. Comparative study of the antimicrobial activity of Selenium Nanoparticles with different Surface Chemistry and structure. Front Bioeng Biotechnol. 2021;8:624621. https://doi.org/10.3389/fbioe.2020.624621.

43. Hasanin M, Al Abboud MA, Alawlaqi MM, Abdelghany TM, Hashem AH. Ecofriendly synthesis of Biosynthesized Copper nanoparticles with Starch-based Nanocomposite: Antimicrobial, antioxidant, and Anticancer activities. Biol Trace Elem Res. 2022;200(5):2099–112. https://doi.org/10.1007/s12011-021-02812-0.

44. Platania V, Kaldeli-Kerou A, Karamanidou T, Kouki M, Tsouknidas A, Chatzinikolaidou M. Antibacterial Effect of Colloidal Suspensions Varying in silver nanoparticles and ions concentrations. Nanomaterials. 2022;12(1):31.

45. Amr M, Abu-Hussien SH, Ismail R, Aboubakr A, Wael R, Yasser M, Hemdan B, El-Sayed SM, Bakry A, Ebeed NM, Elhariry H, Galal A, Abd-Elhalim BT. Utilization of biosynthesized silver nanoparticles from Agaricus Bisporus extract for food safety application: synthesis, characterization, antimicrobial efficacy, and toxicological assessment. Sci Rep. 2023;13(1):15048. https://doi.org/10.1038/s41598-023-42103-3.

46. Hwang I-s, Hwang JH, Choi H, Kim K-J, Lee DG. Synergistic effects between silver nanoparticles and antibiotics and the mechanisms involved. J Med Microbiol. 2012;61(12):1719–26. https://doi.org/10.1099/jmm.0.047100-0.

47. Omanović-Mikličanin E, Badnjević A, Kazlagić A, Hajlovac M. Nanocomposites: a brief review. Health Technol. 2020;10(1):51–9. https://doi.org/10.1007/s12553-019-00380-x.

48. Salem SS, Fouda A. Green Synthesis of Metallic Nanoparticles and their prospective biotechnological applications: an overview. Biol Trace Elem Res. 2021;199(1):344–70. https://doi.org/10.1007/s12011-020-02138-3.

49. Rahimi M, Noruzi EB, Sheykhsaran E, Ebadi B, Kariminezhad Z, Molaparast M, Mehrabani MG, Mehramouz B, Yousefi M, Ahmadi R, Yousefi B, Ganbarov K, Kamounah FS, Shafiei-Irannejad V, Kafil HS. Carbohydrate polymer-based silver nanocomposites: recent progress in the antimicrobial wound dressings. Carbohydr Polym. 2020;231: 115696. https://doi.org/10.1016/j.carbpol.2019.115696.

50. Salem SS. Baker's yeast-mediated silver nanoparticles: Characterisation and Antimicrobial Biogenic Tool for suppressing pathogenic microbes. BioNanoScience. 2022;12(4):1220–9. https://doi.org/10.1007/s12668-022-01026-5.

51. Zhang F, Li X, Wei Y. Selenium and Selenoproteins in Health. Biomolecules. 2023;13(5): 799.

52. Gannoruwa A, Ariyasinghe B, Bandara J. The mechanism and material aspects of a novel Ag2O/TiO2 photocatalyst active in infrared radiation for water splitting. Catal Sci Technol. 2016;6(2):479–87. https://doi.org/10.1039/C5CY01002K.

53. Salem SS. Bio-fabrication of Selenium nanoparticles using Baker's yeast extract and its antimicrobial efficacy on Food Borne pathogens. Appl Biochem Biotechnol. 2022;194(5):1898–910. https://doi.org/10.1007/s12010-022-03809-8.

54. Said A, Abu-Elghait M, Atta HM, Salem SS. Antibacterial activity of Green Synthesized Silver nanoparticles using Lawsonia inermis against common pathogens from urinary tract infection. Appl Biochem Biotechnol. 2024;196(1):85–98. https://doi.org/10.1007/s12010-023-04482-1.

55. Mohsin M, Jawad M, Yameen MA, Waseem A, Shah SH, Shaikh AJ. An insight into the Coating Behavior of Bimetallic Silver and Gold Core-Shell Nanoparticles. Plasmonics. 2020;15(6):1599–612. https://doi.org/10.1007/s11468-020-01166-y.

56. Borah R, Verbruggen SW. Silver–gold bimetallic alloy versus core–Shell nanoparticles: implications for Plasmonic Enhancement and Photothermal Applications. J Phys Chem C. 2020;124(22):12081–94. https://doi.org/10.1021/acs.jpcc.0c02630.

57. Clément M, Abdellah I, Martini C, Fossard F, Dragoe D, Remita H, Huc V, Lampre I. Gold(i)–silver(i)-calix[8]arene complexes, precursors of bimetallic alloyed Au–Ag nanoparticles. Nanoscale Adv. 2020;2(7):2768–73. https://doi.org/10.1039/D0NA00111B.

58. Gopinath K, Kumaraguru S, Bhakyaraj K, Mohan S, Venkatesh KS, Esakkirajan M, Kaleeswarran P, Alharbi NS, Kadaikunnan S, Govindarajan M, Benelli G, Arumugam A. Green synthesis of silver, gold and silver/gold bimetallic nanoparticles using the Gloriosa superba leaf extract and their antibacterial and antibiofilm activities. Microb Pathog. 2016;101:1–11. https://doi.org/10.1016/j.micpath.2016.10.011.

59. Loza K, Heggen M, Epple M. Synthesis, structure, properties, and applications of bimetallic nanoparticles of noble metals. Adv Funct Mater. 2020;30(21): 1909260.

60. Castro-Longoria E, Vilchis-Nestor AR, Avalos-Borja M. Biosynthesis of silver, gold and bimetallic nanoparticles using the filamentous fungus Neurospora Crassa. Colloids Surf B. 2011;83(1):42–8. https://doi.org/10.1016/j.colsurfb.2010.10.035.

61. Garcia PRAF, Prymak O, Grasmik V, Pappert K, Wlysses W, Otubo L, Epple M, Oliveira CLP. An in situ SAXS investigation of the formation of silver nanoparticles and bimetallic silver–gold nanoparticles in controlled wet-chemical reduction synthesis. Nanoscale Adv. 2020;2(1):225–38. https://doi.org/10.1039/C9NA00569B.

62. Govindaraju K, Basha SK, Kumar VG, Singaravelu G. Silver, gold and bimetallic nanoparticles production using single-cell protein (Spirulina platensis) Geitler. J Mater Sci. 2008;43(15):5115–22. https://doi.org/10.1007/s10853-008-2745-4.

63. Zou X, Ying E, Dong S. Preparation of novel silver–gold bimetallic nanostructures by seeding with silver nanoplates and application in surface-enhanced Raman scattering. J Colloid Interface Sci. 2007;306(2):307–15. https://doi.org/10.1016/j.jcis.2006.10.084.

64. Han SW, Kim Y, Kim K. Dodecanethiol-Derivatized Au/Ag Bimetallic Nanoparticles: TEM, UV/VIS, XPS, and FTIR Analysis. Journal of Colloid and Interface Science. 1998;208(1):272–8. https://doi.org/10.1006/jcis.1998.5812.

65. Lomelí-Marroquín D, Medina Cruz D, Nieto-Argüello A, Vernet Crua A, Chen J, Torres-Castro A, Webster TJ, Cholula-Díaz JL. Starch-mediated synthesis of mono-and bimetallic silver/gold nanoparticles as antimicrobial and anticancer agents. Int J Nanomed. 2019;14:2171–90.

66. Baraka A, Dickson S, Gobara M, El-Sayyad GS, Zorainy M, Awaad MI, Hatem H, Kotb MM, Tawfic AF. Synthesis of silver nanoparticles using natural pigments extracted from Alfalfa leaves and its use for antimicrobial activity. Chem Pap. 2017;71(11):2271–81. https://doi.org/10.1007/s11696-017-0221-9.

67. Awed AS, El-Sayyad GS, El-ghandour A, Hameed MFO, Abdel Maksoud MIA, El-Batal AI, Obayya SSA. Unveiling antimicrobial activity of Metal Iodide (CuI, AgI, and PbI2) nanoparticles: towards Biomedical surfaces Applications. J Cluster Sci. 2021;32(1):1–16. https://doi.org/10.1007/s10876-019-01744-z.

68. Hammad EN, Salem SS, Mohamed AA, El-Dougdoug W. Environmental Impacts of Ecofriendly Iron Oxide Nanoparticles on Dyes Removal and

Elkady *et al. BMC Microbiology*   (2024) 24:78

Page 17 of 17

Antibacterial Activity. Appl Biochem Biotechnol. 2022;194(12):6053–67. https://doi.org/10.1007/s12010-022-04105-1.

69. Al-Zahrani FAM, Salem SS, Al-Ghamdi HA, Nhari LM, Lin L, El-Shishtawy RM. Green Synthesis and Antibacterial Activity of Ag/Fe2O3 Nanocomposite Using Buddleja lindleyana Extract. Bioengineering. 2022;9(9):452. https://doi.org/10.3390/bioengineering9090452.

70. Al-Rajhi AM, Salem SS, Alharbi AA, Abdelghany TM. Ecofriendly synthesis of silver nanoparticles using Kei-apple (Dovyalis caffra) fruit and their efficacy against cancer cells and clinical pathogenic microorganisms. Arab J Chem. 2022;15(7):103927. https://doi.org/10.1016/j.arabjc.2022.103927.

71. Salem SS. A mini review on green nanotechnology and its development in biological effects. Arch Microbiol. 2023;205(4):128. https://doi.org/10.1007/s00203-023-03467-2.

72. Abdallah OM, El-Baghdady KZ, Khalil MMH, El Borhamy MI, Meligi GA. Antibacterial, antibiofilm and cytotoxic activities of biogenic polyvinyl alcohol-silver and chitosan-silver nanocomposites. J Polym Res. 2020;27(3):74. https://doi.org/10.1007/s10965-020-02050-3.

73. Kanniah P, Chelliah P, Thangapandi JR, Gnanadhas G, Mahendran V, Robert M. Green synthesis of antibacterial and cytotoxic silver nanoparticles by Piper nigrum seed extract and development of antibacterial silver based Chitosan Nanocomposite. Int J Biol Macromol. 2021;189:18–33. https://doi.org/10.1016/j.ijbiomac.2021.08.056.

74. Asghar MA, Yousuf RI, Shoaib MH, Asghar MA. Antibacterial, anticoagulant and cytotoxic evaluation of biocompatible nanocomposite of chitosan loaded green synthesized bioinspired silver nanoparticles. Int J Biol Macromol. 2020;160:934–43. https://doi.org/10.1016/j.ijbiomac.2020.05.197.

75. Jayeoye TJ, Nwabor OF, Rujiralai T. Synthesis of highly stable and dispersed silver nanoparticles/poly(vinyl alcohol-co-ethylene glycol)/poly(3-aminophenyl boronic acid) nanocomposite: characterization and antibacterial, hemolytic and cytotoxicity studies. J Ind Eng Chem. 2020;89:288–300. https://doi.org/10.1016/j.jiec.2020.05.025.

76. Upadhyay J, Kumar A, Gogoi B, Buragohain AK. Antibacterial and hemolysis activity of polypyrrole nanotubes decorated with silver nanoparticles by an in-situ reduction process. Mater Sci Engineering: C. 2015;54:8–13. https://doi.org/10.1016/j.msec.2015.04.027.

77. Dj MG, Vinaykiya M, Dutta VVB, Pawar S, Raghavendra RVB. Screening of Antibacterial and Antioxidant Activity of Biogenically Synthesized Silver Nanoparticles from Alternaria alternata, Endophytic Fungus of Dendrophthoe falcata-a Parasitic Plant. BioNanoScience. 2022;12(1):128–41. https://doi.org/10.1007/s12668-021-00932-4.

78. Elbasuney S, Yehia M, Ismael S, Al-Hazmi NE, El-Sayyad GS, Tantawy H. Potential impact of reduced Graphene Oxide Incorporated Metal Oxide nanocomposites as Antimicrobial, and Antibiofilm agents against pathogenic microbes: bacterial protein leakage reaction mechanism. J Cluster Sci. 2023;34(2):823–40. https://doi.org/10.1007/s10876-022-02255-0.

79. Ahmad W, Shams S, Ahmad A, Wei Y, Yuan Q, Khan AU, Khan MS, Ur Rahman A, Iqbal M. Synthesis of selenium–silver nanostructures with enhanced antibacterial, photocatalytic and antioxidant activities. Appl Nanosci. 2020;10(4):1191–204. https://doi.org/10.1007/s13204-019-01213-z.

80. Abd-Elraoof WA, Tayel AA, El-Far SW, Walid Abukhatwah OM, Diab AM, Abonama OM, Assas MA, Abdella A. Characterization and antimicrobial activity of a chitosan-selenium nanocomposite biosynthesized using Posidonia oceanica. RSC Adv. 2023;13(37):26001–14. https://doi.org/10.1039/D3RA04288J.

81. Trzcińska-Wencel J, Wypij M, Rai M, Golińska P. Biogenic nanosilver bearing antimicrobial and antibiofilm activities and its potential for application in agriculture and industry. Front Microbiol. 2023;14:14. https://doi.org/10.3389/fmicb.2023.1125685.

82. Arsène MMJ, Viktorovna PI, Alla M, Mariya M, Nikolaevitch SA, Davares AKL, Yurievna ME, Rehailia M, Gabin AA, Alekseevna KA, Vyacheslavovna YN, Vladimirovna ZA, Svetlana O, Milana D. Antifungal activity of silver nanoparticles prepared using Aloe vera extract against Candida albicans. Veterinary World. 2023;16(1):18–26. https://doi.org/10.14202/vetworld.2023.18-26.

83. Chatterjee K, Taneja J, Khullar S, Pandey AK. Antifungal activity of silver nanoparticles on fungal isolates from patients of suspected mucormycosis. Int Microbiol. 2023;26(1):143–7. https://doi.org/10.1007/s10123-022-00280-7.

84. Hashem AH, Salem SS. Green and ecofriendly biosynthesis of selenium nanoparticles using Urtica dioica (stinging nettle) leaf extract:

antimicrobial and anticancer activity. Biotechnol J. 2022;17(2): 2100432. https://doi.org/10.1002/biot.202100432.

85. Soliman MKY, Abu-Elghait M, Salem SS, Azab MS. Multifunctional properties of silver and gold nanoparticles synthesis by Fusarium Pseudonygamai. Biomass Convers Biorefinery. 2022. https://doi.org/10.1007/s13399-022-03507-9.

86. Soliman MKY, Salem SS, Abu-Elghait M, Azab MS. Biosynthesis of silver and gold nanoparticles and their efficacy towards Antibacterial, Antibiofilm, cytotoxicity, and antioxidant activities. Appl Biochem Biotechnol. 2023;195(2):1158–83. https://doi.org/10.1007/s12010-022-04199-7.

87. Bellisario D, Santo L, Quadrini F, Hassiba M, Bader N, Chowdhury SH, Hassan MK, Zughaier SM. Cytotoxicity and antibiofilm activity of Silver-Polypropylene Nanocomposites. Antibiotics. 2023;12(5): 924.

88. El-Behery RR, El-Sayed E-SR, El-Sayyad GS. Gamma rays-assisted bacterial synthesis of bimetallic silver-selenium nanoparticles: powerful antimicrobial, antibiofilm, antioxidant, and photocatalytic activities. BMC Microbiol. 2023;23(1):224. https://doi.org/10.1186/s12866-023-02971-1.

Publisher's Note

Springer Nature remains neutral with regard to jurisdictional claims in published maps and institutional affiliations.